Mon. Not. R. Astron. Soc. **000**, 000–000 (0000) Printed 16 August 2007 (MN LATEX style file v2.2)

The nature of X-ray selected EROs

J. A. Stevens[1,2], M. J. Page[2], R. J. Ivison[1], Ian Smail[3], I. Lehmann[4,5], G. Hasinger[4,5] and G. Szokoly[4,5]

[1] *Astronomy Technology Centre, Royal Observatory, Blackford Hill, Edinburgh EH9 3HJ*
[2] *Mullard Space Science Laboratory, University College London, Holmbury St. Mary, Dorking, Surrey, RH5 6NT*
[3] *Department of Physics, University of Durham, South Road, Durham DH1 3LE*
[4] *Astrophysikalisches Institut Potsdam (AIP), An der Sternwarte 16, 14482 Potsdam, Germany*
[5] *Max-Plank-Institut Für extraterrestrische Physik, Giessenbachstrasse PF 1312, 85748 Garching bei Muenchen, Germany*

draft 1.0

ABSTRACT

We report on the X-ray, optical, near-infrared, submillimetre and radio properties of five Extremely Red Objects (EROs) selected at X-ray wavelengths by *XMM-Newton* in the Lockman Hole field. They all have enough counts in the X-ray band to allow spectral fitting: four are most probably obscured, Compton-thin AGN with redshift dependent absorbing column densities of $10^{22} - 10^{24}$ cm^{-2}, whilst the fifth is best fitted by a thermal spectrum and is likely to be a massive elliptical galaxy in a deep gravitational potential. Their optical/near-infrared colours and sizes suggest that X-ray selected EROs comprise a mixture of dusty 'starburst' galaxies and non-dusty galaxies that are dominated by either star-light or light from an active nucleus. The colour diagnostics are supported by the submillimetre and radio data: the two AGN with 'starburst' colours have submillimetre or radio flux densities that imply large star-formation rates, whilst those with 'elliptical' colours do not. The one source detected in the submillimetre waveband has narrow emission lines at a redshift of 1.45. Although the bulk of its radio emission originates from processes other than star formation, it is most probably a radio-quiet ultraluminous infrared galaxy.

Key words: galaxies: active - infrared: galaxies - X-rays: galaxies - Radio continuum: galaxies - submillimetre

1 INTRODUCTION

The recent launch of the *XMM-Newton* and *Chandra* observatories has produced considerable interest in the nature of the faint extragalactic X-ray population. In particular, the X-ray background at $2 - 10$ keV energies has been almost completely resolved for the first time by these facilities. Synthesis models for the hard X-ray background, which require a large population of heavily obscured AGN (e.g. Setti & Woltjer 1989), predict that about 85 per cent of the accretion power in the Universe is absorbed (Fabian & Iwasawa 1999). This absorbed energy is expected to be re-emitted in the infrared–millimetre waveband.

One of the most interesting discoveries from the previous, *Rosat*, era was that a small number of faint X-ray sources were identified with extremely red optical/infrared counterparts (Newsam et al. 1997; Lehmann et al. 2001). Extremely red objects (EROs) were discovered more than a decade ago (Elston, Rieke & Rieke 1988) but their connection with the broad extragalactic population is only just becoming clear. It is thought that the population is bimodal; EROs are either (1) elliptical galaxies at high-redshift ($z \sim 1$), their red colours being produced by an evolved stellar population, or (2) they are starburst galaxies at high-redshift ($z > 1$) and their red colours are produced by the suppression of UV light from young stars by dust. However, there is growing evidence that the population of EROs might be more diverse than originally thought with several sources showing evidence of AGN activity (Smith et al. 2001; Pierre et al. 2001; Afonso et al. 2001). In a recent study, the X-ray colours of EROs in the *Chandra* Deep Field North suggest that 9 out of 13 of them have X-ray emission from obscured AGN (Alexander et al. 2002). The other 4 are likely to be a mixture of low-luminosity AGNs, normal ellipticals and starbursts.

The first deep survey made with *XMM-Newton* was a 100 ks observation of the Lockman Hole (Hasinger et al. 2001). Follow-up observations revealed a population of EROs. Most of these EROs have high X-ray-to-optical flux ratios indicating the presence of an obscured AGN (Mainieri et al. 2002). The large collecting area of *XMM-Newton* makes it possible to examine their X-ray spectra on a case by case basis, providing an excellent opportunity to determine the origin of their X-ray emission, and thereby investigate the role of buried AGN in these objects. To elucidate the connection between the X-ray and global properties of EROs we here report on radio, millimetre, submillimetre and optical/near-infrared ob-

Table 1. Source names and coordinates of optical counterparts. Sources with $Rosat$ numbers were detected in the previous deep survey of the Lockman Hole. Source number 84 is discussed by Lehmann et al. (2001).

ero#	Source name	RA J2000	Dec J2000	*Rosat* number
ero1	XMMUJ $105216.9+572017$	10 52 16.97	+57 20 17.1	84
ero2	XMMUJ $105348.1+572817$	10 53 48.05	+57 28 16.7	...
ero3	XMMUJ $105146.5+573037$	10 51 46.58	+57 30 35.1	...
ero4	XMMUJ $105225.5+572551$	10 52 25.29	+57 25 50.7	491
ero5	XMMUJ $105255.5+571950$	10 52 55.50	+57 19 51.0	438

Table 2. X-ray fluxes in the various bands. Column 2 has the source circle, ø, used to extract the X-ray spectrum. Column 3 has the total source counts within this circle.

Name	ø arcsec	counts [0.2 − 12 keV]	$S_{0.2-0.5\,\mathrm{keV}}$	$S_{0.5-2.0\,\mathrm{keV}}$	$S_{2.0-5.0\,\mathrm{keV}}$	$S_{5.0-12\,\mathrm{keV}}$
			10^{-16}erg cm^{-2} s^{-1}			
ero1	30.0	504	0.64 ± 5.32	56.68 ± 4.07	170.42 ± 11.45	378.18 ± 70.41
ero2	19.0	153	0.00 ± 4.48	24.97 ± 3.24	53.30 ± 7.71	224.09 ± 62.78
ero3	14.5	132	17.27 ± 3.26	32.30 ± 3.34	19.51 ± 5.01	61.67 ± 45.37
ero4	13.0	244	1.68 ± 1.21	22.11 ± 2.27	60.38 ± 5.77	180.43 ± 37.51
ero5	22.4	88	1.53 ± 1.40	17.85 ± 2.90	22.17 ± 5.75	116.87 ± 57.01

servations of five objects selected from the 100 ks *XMM-Newton* observation of the Lockman Hole.

Throughout this paper we define spectral index, α, as $S_\nu \propto \nu^\alpha$ where S_ν is the flux density at frequency ν. We assume $H_0 = 50$ km s^{-1} Mpc^{-1}, and $q_0 = 0.5$ throughout unless otherwise stated.

2 SAMPLE

Our sample comprises five out of six of the reddest sources (those satisfying $R - K' > 6$) in the 100 ks *XMM-Newton* observation of the Lockman Hole (Hasinger et al. 2001). Due to telescope time constraints, the other source was not observed in the submillimetre band and, likewise, lacks good quality imaging data in the near-infrared. For clarity it is not discussed in this paper. In Table 1 we give the names and coordinates of the sources; three of them were detected in the *Rosat* Deep Survey although they were not spectroscopically identified (Hasinger et al. 1998; Lehmann et al. 2001). However, ero5 now has a measured redshift of $z = 1.45$ from the detection of narrow Hα in a K-band spectrum and narrow [O III]λ5007 in a H-band spectrum, both taken at the Subaru telescope (PIs: Masayuki Akiyama, Patrick Henry). In addition, ero1, the hardest source in the *Rosat* sample has a photometric redshift of $z \sim 2.7$, although redshifts as low as 1.5 are statistically acceptable (Lehmann et al. 2001). However, photometric redshifts should be treated with caution given that an AGN might contribute to the optical/near-infrared light (see Sections 4.2 and 5).

In the part of the *XMM-Newton* Lockman field that has been imaged in the K band there are 151 objects that satisfy $R-K' > 6$ and $K \leq 20$. Of these 6 (4 per cent) have been detected as X-ray sources.

3 OBSERVATIONS

3.1 X-ray observations

The Lockman Hole was observed five times by the *XMM-Newton* EPIC cameras during April and May 2000, as described in Hasinger et al. (2001). The data presented here are the same as those used by Hasinger et al. (2001) but we have reprocessed the data with the *XMM-Newton* Science Analysis System (SAS) version 5.3, using the latest calibration data. The events were transformed to a common astrometric frame by cross-correlating the source positions derived from each of the observations with the optical counterpart positions from the previous *Rosat* HRI survey (Lehmann et al. 2001).

Images and exposure maps were formed for each observation in four energy bands: $0.2-0.5$ keV, $0.5-2.0$ keV, $2.0-5.0$ keV and $5.0 - 12.0$ keV; photons with energies close to those of the strong instrumental emission lines (Lumb et al. 2002) were excluded from the images. Background maps for each observation and each energy band were created by maximum-likelihood fitting of uniform vignetted and unvignetted components to the images after sources had been excised. Images, exposure maps and background maps from the different observations were then combined. The images in the four energy bands were simultaneously searched for sources using the SAS tasks EBOXDETECT and EMLDETECT. To optimize the background determination we performed several iterations of source detection and background fitting. Count rates were converted to fluxes assuming a power law spectrum with $\alpha = -0.7$.

For spectral analysis we obtained source counts from circles of between 13 arcsec and 30 arcsec radius centred on the source positions given in Table 2. The sizes of the source circles were determined primarily by the need to avoid contamination by other nearby sources. Background counts were obtained from annular regions of diameter 2 arcmin around the source positions; sources with more than 40 counts were excised from the background regions. For the MOS spectra, single, double and triple event patterns were used, while in the PN spectra single and double events were used. Events with nominal energy < 0.2 keV were excluded be-

Table 3. Optical and near-infrared photometry, colours and half-light radii ($r_{\rm hl}$)

Name	R mag	J mag	$t_{\rm int}$ (J) sec	K mag	$t_{\rm int}$ (K) sec	$R-K$ mag	$J-K$ mag	$r_{\rm hl}$ arcsec
ero1[a]	25.5	21.85 ± 0.12	9720	19.45 ± 0.04	3240	6.1 ± 0.05	2.40 ± 0.13	0.12 ± 0.08
ero2	25.5	21.38 ± 0.08	6480	18.91 ± 0.03	2160	6.6 ± 0.05	2.47 ± 0.07	0.16 ± 0.06
ero3	25.6	21.75 ± 0.10	12960	19.80 ± 0.05	4860	5.8 ± 0.06	1.95 ± 0.11	0.43 ± 0.07
ero4	24.6	20.44 ± 0.05	9180	18.79 ± 0.03	2160	5.8 ± 0.05	1.65 ± 0.06	0.29 ± 0.05
ero5	24.2	20.90 ± 0.15	2160	18.29 ± 0.05	1620	5.9 ± 0.06	2.61 ± 0.16	0.00 ± 0.08

[a]Lehmann et al. (2001) find $K = 19.4 \pm 0.1$ and $J = 21.7 \pm 0.2$ for ero1, consistent with the values presented here.

Table 4. Radio positions measured from the 1.4-GHz VLA map, radio and submillimetre flux measurements. The values quoted in columns 4 and 5 are offsets between the radio positions and those quoted in Table 2. Column 6 has the source size measured at 1.4 GHz; the measurements have not been deconvolved with the 1.4 arcsec beam.

Name	RA J2000	Dec J2000	$\lvert\Delta$RA$\rvert$ arcsec	$\lvert\Delta$Dec$\rvert$ arcsec	θ_{FWHM} arcsec	1.4 GHz μJy	4.9 GHz μJy	450 μm mJy	850 μm mJy
ero1	10 52 16.90	57 20 17.2	0.6	0.1	1.4 ± 0.1	113 ± 12	104 ± 39	2.2 ± 10.5	-1.4 ± 1.4
ero2	...	...	...	...	...	$3\sigma < 27$	...	-3.6 ± 8.4	1.8 ± 1.0
ero3	...	...	...	...	...	$3\sigma < 16$	$3\sigma < 43$	10.6 ± 7.5	1.8 ± 1.1
ero4	10 52 25.44	57 25 51.1	1.2	0.4	1.6 ± 0.4	31 ± 13	$3\sigma < 35$	-9.2 ± 22.4	-2.5 ± 1.6
ero5	10 52 55.32	57 19 50.4	1.5	0.6	1.43 ± 0.01	2990 ± 100	1090 ± 70	16.7 ± 9.8	4.3 ± 1.0

cause the EPIC responses are uncertain at such low energies. We further excluded events with nominal energy < 0.4 keV in PN because of the increased noise levels when double events are selected in this energy range. Response matrices for each source were produced using the SAS tasks RMFGEN and ARFGEN. Photons from channels contaminated by the strong instrumental fluorescent emission lines (Al K in MOS and Cu K in PN) were excluded from both source and background spectra. Spectra from the five observations and three EPIC cameras were combined by summing the counts from channels with the same nominal energy range. Background spectra were summed in the same fashion. The response matrices were combined by averaging the effective areas of the individual response matrices for each channel and each energy range. The procedure is described in detail in Page, Davis & Salvi (2003). The resultant spectra were grouped to a minimum of 20 counts per bin before spectral fitting.

3.2 Near-infrared/optical observations

We used the near-infrared camera UFTI on the 3.8-m United Kingdom InfraRed Telescope (UKIRT) to make images at J and K (and H for ero5 only; $H = 19.30 \pm 0.15$ mag) on 2001 February 17 and 2001 March $12-16$. UFTI is a 1024×1024 InSb imager with 0.091 arcsec pixels. Data were taken in periods of good atmospheric transparency and with seeing of $0.4-1.1$ arcsec. We used a 3×3 grid of dithered positions for each image, allowing the construction of a sky frame for flatfielding. Integration times are given in Table 3. Calibration was obtained by observing a selection of UKIRT faint standards (Hawarden et al. 2001) on each night.

The data were analysed with the ORAC-DR data reduction pipeline which automates the dark subtraction, flat-fielding, resampling and despiking steps. The resulting mosaics were coadded as required with the STARLINK CCDPACK tasks CCDALIGN and MAKEMOS. We obtained secure identifications by calibrating the data astrometrically using bright stars in the images. Magnitudes, calculated in 2 arcsec diameter apertures, are given in Table 3 along with $R-K$ and $J-K$ colours.

3.3 Millimetre and submillimetre observations

Submillimetre observations were made at the James Clerk Maxwell Telescope (JCMT) on the 2001 January $22-24$. We used SCUBA in photometry mode (see Holland et al. 1999) to make sensitive continuum observations in the 850- and 450-μm atmospheric passbands. The measured beam sizes at these wavelengths are approximately 14.5 and 8.0 arcsec respectively. The adopted chop throw was 45 arcsec in azimuth. Atmospheric transparency and stability were in the top quartile of conditions experienced on Mauna Kea; the zenith opacity was monitored with skydips yielding values of $0.18-0.19$ and $0.8-0.9$ at 850 and 450 μm respectively. Telescope pointing accuracy was checked on the nearby blazar $1044+719$ at $25-45$ min intervals. Local pointing offsets were in all cases better than 2 arcsec.

Data reduction was performed in the standard manner using the STARLINK package SURF (Jenness & Lightfoot 1998), and flux calibration was made with respect to the JCMT primary calibrator, Mars. Calibration uncertainties are estimated to be $\sim 5-10$ per cent at 850 μm and $\sim 15-20$ per cent at 450 μm. The resulting rms noise limits on our coadded photometric observations give noise equivalent flux densities of $\sim$ 80 and $\sim$ 800 mJy.Hz$^{-1/2}$ at 850 and 450 μm respectively, entirely consistent with both predicted and previously measured values in similar weather conditions. Submillimetre flux densities are given in Table 4

One source, ero5, was observed at the IRAM 30-m telescope during March 2001 with the MPifR 37-channel bolometer array operating at 1.25 mm. The integration time was 3314 secs with the array operating in ON/OFF mode. The observing and data reduction strategy is analogous to that used with SCUBA at the JCMT.

3.4 Radio observations

The Lockman field was mapped with the National Radio Astronomy Observatory's (NRAO) Very Large Array (VLA).

At 1.4 GHz, interference and the presence of bright sources in the primary beam meant that we had to use the spectral-line correlator mode, recording data every 5 s in 3.25 MHz channels, 28 in total, including left-circular and right-circular polarizations. 3C 84 and 3C 286 were used for flux calibration. The phase/amplitude calibrator, 1035+564, was observed every hour. A total of 75 h of integration was obtained — 70 h in A configuration; 5 h in B configuration. The lengthy data reduction procedure is described in detail by Ivison et al. (2002). The resulting map has a noise level of $\sim 4-5\,\mu$Jy beam^{-1} with 1.4 arcsec resolution.

At 4.9 GHz, data were taken in the standard continuum correlator mode in C configuration, with a total bandwidth of 100 MHz, and reduced according to the standard AIPS recipes. The resulting map has a noise level of $\sim 13\,\mu$Jy beam^{-1} with 5 arcsec resolution.

Radio source positions measured at 1.4 GHz, together with flux densities and upper limits, are given in Table 4.

4 RESULTS

4.1 X-ray properties

The X-ray fluxes of the EROs, derived from multi-band source detection and parameterization are listed in Table 2. It is immediately clear that ero3 is much softer than the other EROs: it is the only source detected below 0.5 keV but it is the weakest source at energies higher than 2 keV. As expected, this difference is borne out by spectral fitting.

Initially, each of the ERO spectra were fitted with a power law model, absorbed only by the Galactic column in the direction of the Lockman Hole (6×10^{19} cm^{-2}; Lockman et al. 1986). The results of these fits (and those discussed below) are given in Table 5 and are shown graphically in Fig. 1. The power law model is an extremely poor fit to ero1 and ero2, and the fitted power law indices for ero1, ero2 and ero4 are much harder than the spectra of typical unobscured AGN. The power law fits to ero1, ero2 and ero4 also result in strong residuals which are characteristic of photoelectric absorption: an excess of counts above 1 keV, and a deficit of counts below 1 keV. We have therefore re-fitted the spectra using an absorbed power law model, with the redshift and column density of the absorbing medium as free parameters; Galactic absorption was included as before. This results in much better fits to the spectra of ero1, ero2, ero4 and ero5. In all four cases the improvement in χ^2/ν (here ν is the number of data points minus the number of free parameters) is significant at > 99 per cent according to the F-test, and the intrinsic power-law spectral indices are now consistent with those found in normal AGN. The derived column densities shown in Fig. 2 depend heavily on redshift, but probably lie somewhere between 10^{22} and 10^{24} cm^{-2}. Finally, to see if the X-ray emission could have a thermal origin, we have attempted to fit the spectra using a Mekal optically-thin thermal plasma model with Galactic absorption. We assumed Solar abundances for the plasma but its redshift was a free parameter in the fits. This model is a poor fit regardless of redshift for ero1, ero2 and ero4, and for ero5 it is a poorer fit than the absorbed power law model. For ero3, however, it is a slightly better fit than an absorbed or unabsorbed power law. The acceptable range of temperatures and redshifts for this source are shown in Fig. 3. For each ERO, the best-fit model is overplotted on the observed spectrum in Fig. 1.

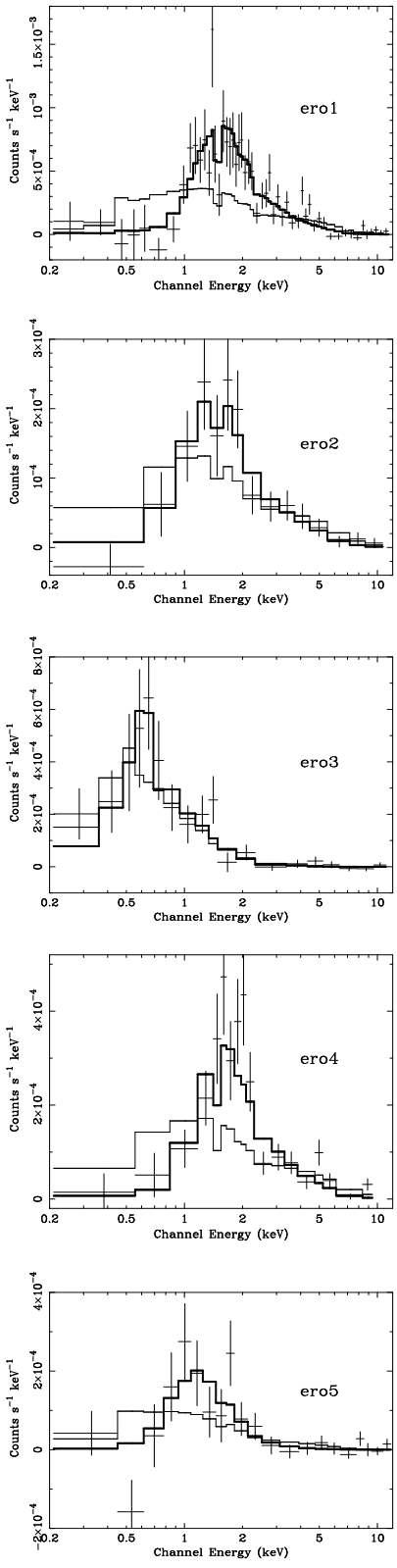

Figure 1. X-ray spectra of the five EROs. In each case, the thin line shows the best power law model folded through the response, while the bold line shows the overall best fit model (a thermal plasma for ero3, an absorbed power law for the other EROs) folded through the response. The drop in response below 0.4 keV is due to the exclusion of the PN data in this energy range (see Section 3.1).

Table 5. Model fits to the ERO X-ray spectra. The energy index α is defined here (and throughout the paper) as $S_\nu \propto \nu^\alpha$. The errors are quoted at 95% confidence for one interesting parameter (i.e. $\Delta\chi^2 = 4$); an '*' indicates that the fit parameter reaches the limit on its allowed range before $\Delta\chi^2 = 4$. 'Prob' is the probability of obtaining the observed χ^2/ν or greater if the data were drawn from the model.

Source	power law			absorbed powerlaw			thermal plasma		
	α	χ^2/ν	Prob	α	χ^2/ν	Prob	kT (keV)	χ^2/ν	Prob
ero1	$0.3^{+0.2}_{-0.1}$	162.3/51	1.6×10^{-13}	$-1.7^{+0.5}_{-0.6}$	57.5/49	0.19	100^{+*}_{-42}	199.0/51	1.1×10^{-19}
ero2	$0.3^{+0.3}_{-0.3}$	22.1/13	5.4×10^{-2}	$-0.8^{+0.8}_{-1.0}$	5.8/11	0.88	100^{+*}_{-78}	38.2/12	1.4×10^{-4}
ero3	$-1.5^{+0.5}_{-0.6}$	16.4/17	0.50	$-1.8^{+0.8}_{-3.9}$	15.7/15	0.40	$1.9^{+1.2}_{-0.6}$	14.0/16	0.60
ero4	$0.3^{+0.3}_{-0.2}$	62.9/16	1.7×10^{-7}	$-1.5^{+0.8}_{-1.2}$	24.3/14	4.2×10^{-2}	100^{+*}_{-40}	90.9/15	6.8×10^{-13}
ero5	$-0.2^{+0.7}_{-0.6}$	32.5/19	2.7×10^{-2}	$-2.6^{+1.6}_{-3.9}$	18.5/17	0.356	$1.5^{+*}_{-0.6}$	29.6/18	4.1×10^{-2}

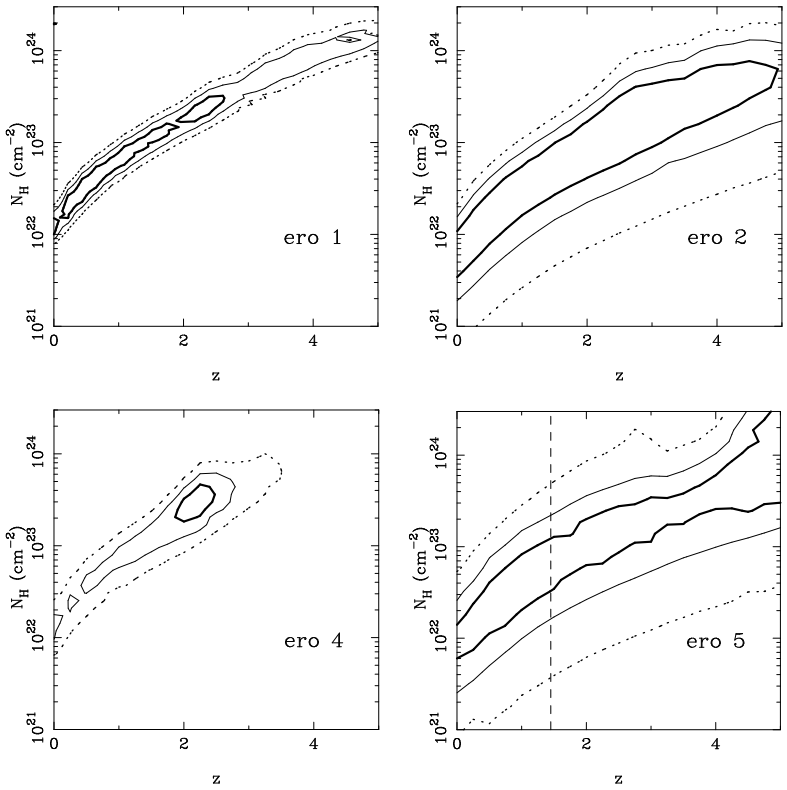

Figure 2. Confidence intervals for the redshift and absorbing column density for those EROs with X-ray spectra that are best fitted by an absorbed power law. The bold solid, thin solid, and dotted contours correspond to 1, 2 and 3 σ respectively. The dashed line on the lower right panel corresponds to $z = 1.45$ for ero5; at 95 per cent confidence level the range of acceptable column densities is $6.2^{+10.5}_{-4.0} \times 10^{22}$.

4.2 Radio to near-infrared properties

In this section we use our multicolour photometric and imaging data to investigate the nature of our five X-ray selected EROs.

Since an old stellar population will show a break in the 4000 Å region whereas a dusty starburst (or dusty AGN) will have a smoother and shallower overall spectrum it has been proposed that the two populations will fall in different regions of, for example, a $R-K$ vs $J-K$ diagram (Pozzetti & Mannucci 2000). The first indications are that this is indeed the case, with known elliptical and starbursting EROs falling in the regions predicted by these spectral synthesis models (Pozzetti & Mannucci 2000). In addition, it has been shown that EROs detected in a very deep radio map (where the radio flux is assumed to be connected with star formation – see below) have redder $J-K$ colours on average than those that were not detected (Smail et al. 2002). In the same study, spectral synthesis models fitted to broad-band photometric data showed that those sources best-fitted by dusty starburst models tended to have redder $J-K$ colours than those fitted by an evolved stellar population (Smail et al. 2002). In Fig. 4 we use our optical and near-infrared photometry to produce a $R-K$ vs $J-K$ colour-colour diagram. Three of the five sources have clear-cut classifications according to this diagnostic tool; ero5 is a dusty 'starburst' source, while ero3 and ero4 are 'ellipticals'. In addition, ero1 may also be dusty but ero2 falls on the boundary between the two classifications.

Small K-band images centred on the EROs are presented in Fig. 5. The images are not deep enough to allow profile fitting but we were able to extract half-light radii ($r_{\rm hl}$) by comparing the EROs with stars in their respective images, i.e. we determined the full width half maximum of the ERO and the best star in the frame, deconvolved them assuming Gaussian sources and then translated the results into half-light radii. The results are presented in Table 3,

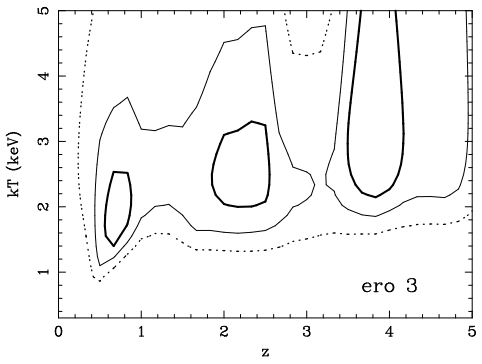

Figure 3. Confidence interval on temperature and redshift for a thermal plasma model fit to the X-ray spectrum of ero3. The bold solid, thin solid, and dotted contours correspond to 1, 2 and 3σ respectively.

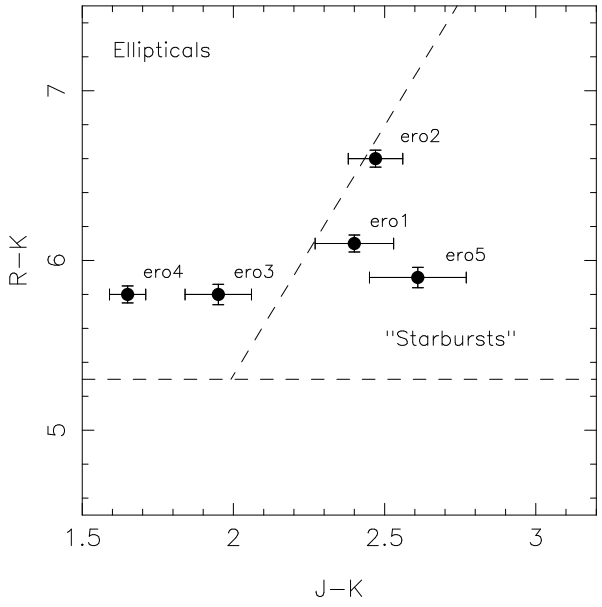

Figure 4. Colour-colour diagram. The diagonal dashed line separates passively evolving elliptical galaxies from dusty 'starburst' galaxies (Pozzetti & Mannucci 2000). Our EROs are chosen to lie above the horizontal dashed line at $R-K>5.3$.

and we plot $r_{\rm hl}$ versus K magnitude in Fig. 6 together with models taken from Roche et al. (2002). These models are based on the size-luminosity relations of local spheroidal (E/S0) and spiral (disk) galaxies combined with passive luminosity evolution. The results for ero3 and ero4 agree with those found above from their photometric colours; they are consistent with passively evolving elliptical or spiral galaxies, ero4 with a $z=1$ E/S0 and ero3 with either a $z=2$ E/S0 or a $z=1$ disk. Inspection of the images shown in Fig. 5 shows that ero3 might have an elongated morphology typical of an inclined spiral galaxy, although its size and morphology might alternatively be ascribed to an ongoing merger. The other three EROs are inconsistent with all of the models - this is particularly the case for ero5 which is indistinguishable from the stars on its image. As a comparison, *Hubble Space Telescope* imaging data (Smith et al. 2002) show that only 3 of 62 K-band selected EROs with $R-K>5.3$ (1/27 with $R-K>6.0$) have sizes smaller than 0.16 arcsec (that of ero2). Similarly, ero1, ero2 and ero5 are smaller than practically all of the 32 $K\leq19.5$ EROs selected from R- and K-band imaging data by Roche et al. (2002).

If any of the X-ray selected EROs are luminous, heavily dust reddened starbursts they will show signatures of star formation in other wavebands. In particular, we expect them to have strong emission in the submillimetre band from warm dust heated by young stars, and synchrotron radiation in the radio band resulting from supernovae. If, instead, the sources are red because they have a redshifted, evolved stellar population, they will not show these characteristics. This simple picture, however, is complicated by the presence of an AGN which can produce synchrotron radiation at radio wavelengths, and at submillimetre wavelengths can heat circumnuclear dust. Of the five sources only one, ero5, is detected at 850 μm with SCUBA (Table 4). Three of them (ero1, ero4 and ero5) are detected at one or both radio frequencies (Table 4). All three of the radio detected sources are unresolved at the 1.4 arcsec resolution of the 1.4-GHz VLA map (Table 4).

We discuss ero5 in detail in Appendix A where we conclude that it is probably a radio-quiet AGN and that the submillimetre emission is from warm dust. We can investigate the heating source of the dust by comparing the bolometric luminosity emitted by the AGN (L_{AGN}) to that emitted in the far-infrared (L_{FIR}). Assuming an intrinsic X-ray spectral index of -1 and using the absorbed power law fit reported in Section 4.1, the flux emitted in the $0.5-2$ keV band, corrected for absorption is $3.0^{+1.7}_{-1.3}\times10^{-15}$ erg s^{-1}. If 3 per cent of the AGN luminosity is emitted in the $0.5-2$ keV band (Elvis et al. 1994) then $\log(L_{AGN})=11.55^{+0.19}_{-0.25}\ L_\odot$ at $z=1.45$. We assume further that ero5 has the same far-infrared spectrum as Mrk 231, an X-ray absorbed AGN in the local Universe with $\log(L_{FIR})=12.59\ L_\odot$ (see Page et al. 2001 and references therein). If observed at $z=1.45$ Mrk 231 would have an 850 μm flux density of 1.9 mJy. Scaling with ero5 we derive $\log(L_{FIR})=12.95\pm0.10\ L_\odot$, large enough to classify ero5 is an ultraluminous infrared galaxy or ULIRG. The ratio $L_{FIR}/L_{AGN}=25^{+13}_{-15}$ suggests that the far-infrared luminosity of ero5 is powered by star formation, in which case the star-formation rate (SFR) can be calculated from SFR(M$_\odot$yr^{-1}) $=L_{FIR}/5.8\times10^9$ (Kennicutt 1998) giving SFR~1500 M$_\odot$yr^{-1}.

The other two sources detected at radio wavelengths are fainter than ero5 by factors of ~20 (ero1) and ~45 (ero4) at 1.4 GHz, and are thus also unlikely to be radio-loud given their similar optical/near-infrared magnitudes. Their radio emission could, however, be associated with strong star formation and/or weak AGN activity. Taking advantage of the opposite (and strong in the submillimetre case) K-corrections in the two bands, a number of studies have used the radio to submillimetre spectral index as a redshift indicator (e.g., Carilli & Yun 1999; Dunne, Clements & Eales 2000). Assuming a 2σ upper limit of 2.8 mJy, ero1 has a spectral index $\alpha^{350}_{1.4}<0.58$ leading to rough redshift constraints $z<1.5$ and $z<1.0$ respectively from the two studies cited above. Similarly, ero4 has $\alpha^{350}_{1.4}<0.83$ leading to $z<3.5$ and $z<2.2$ respectively, and consistent with that deduced from Fig. 6. However, if the AGN contributes to the radio emission then higher redshifts (up to $z=6$ or so) are possible. We can put a rough limit on their SFRs by assuming that all of the radio emission has a starburst origin and that they are at $z=1$. Then, SFR(M$_\odot$yr^{-1}) $=5.9\pm1.8\times10^{-22}L_{1.4\rm GHz}$ where $L_{1.4\rm GHz}$ is the 1.4-GHz luminosity in units of W Hz^{-1} (Yun, Reddy & Condon 2001). The calculated SFRs are ≤340 and ≤90 M$_\odot$yr^{-1} for ero1 and ero4 respectively.

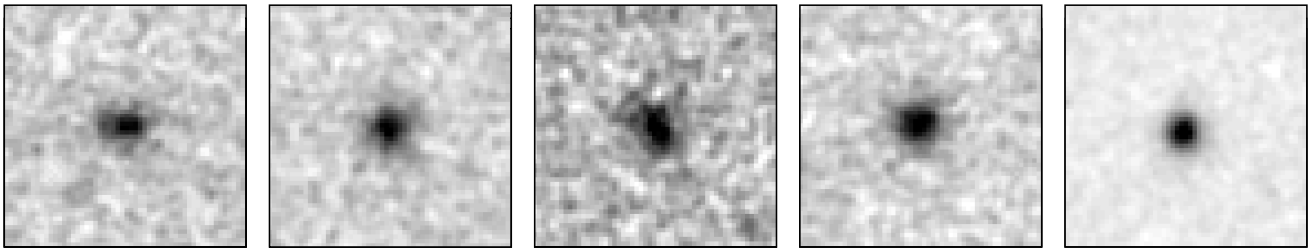

Figure 5. K-band images smoothed with a Gaussian of 2 pixels FWHM. From left to right are ero1, ero2, ero3, ero4 and ero5. Each panel is 5×5 arcsec.

Two sources, ero2 and ero3, are undetected in both the radio and submillimetre bands. Their radio detection limits give SFRs of < 80 and < 50 $\mathrm{M_{\odot}yr^{-1}}$ respectively at $z = 1$.

5 DISCUSSION

The results from the previous section and the proposed source classifications discussed below are summarized in Table 6.

Our X-ray spectral analysis shows that ero1, ero2, ero4 and ero5 almost certainly contain absorbed AGN. The optical/near-infrared colours suggest that absorbed AGN occur in both types of ERO: dust-reddened starbursts (e.g. ero5), and EROs that are dominated by an old stellar population (e.g. ero4). The K-band half-light radius of ero4, as well as the optical/near-infrared colours, are consistent with an early type galaxy at $z \sim 1$ assuming passive luminosity evolution; this suggests that the AGN in this source contributes very little to its optical/near-infrared light.

In contrast to ero4, the two 'dusty starburst' EROs and the source with an ambiguous colour classification (ero2) are unusually compact in the K-band images, suggesting that their near-infrared emission includes a significant contribution from the absorbed AGN. The column densities measured in the X-ray ($< 10^{23}\mathrm{cm}^{-2}$ for $z \sim 1$) do not preclude such a possibility. Indeed, the dust-reddened optical/near-infrared colours of AGN are indistinguishable from the colours of young, massive stellar populations, and therefore it is possible that these three sources were selected as EROs because they contain dust obscured AGN rather than dusty star formation. This potential AGN contribution means that the optical/near-infrared colours alone are not sufficient to determine the nature of the host galaxies in these three objects. However, the submillimetre detection of ero5 suggests that this source *is* a dusty starburst galaxy. In Section 4.2 we argue that it is a ULIRG forming stars at a rate of $\sim 1000 - 1500$ $\mathrm{M_{\odot}yr^{-1}}$. The detection of radio emission from ero1 suggests that this source is also a dusty, star-forming galaxy. However, the lack of any detectable radio or submillimetre emission from ero2 suggests that like ero4, it could be an absorbed AGN hosted by a quiescent, early type galaxy.

It is thus apparent that absorbed AGN are found in both types of ERO: elliptical galaxies at $z \sim 1$ and high-redshift dusty starbursts. EROs such as ero2 and ero4, which correspond to the first type, have properties that are consistent with a normal galaxy containing an AGN which is viewed through an obscuring torus, as expected from AGN unified schemes (Antonucci 1993), and hypothesized in large numbers to explain the X-ray background (e.g. Comastri et al. 1995). In these cases, the dust is located close to the AGN itself, and may be hot. At least two hard X-ray sources discovered by *Chandra* have been shown to exhibit these properties (Wilman, Fabian & Gandhi 2000; see also Deane & Trentham 2001). EROs such as ero1 and ero5, which correspond to the second type, appear to be undergoing vigorous star formation. In these sources some obscuration of the AGN could be due to warm dust and gas which is associated with the star-forming regions, rather than an obscuring torus. Such sources may be AGN at an earlier evolutionary phase than the unobscured AGN population (e.g. Fabian 1999). Whatever the host galaxy, if the AGN makes a significant contribution to the K-band flux the position of the source on the colour-colour diagram could be shifted relative to position of the host galaxy, and we caution against applying photometric redshift techniques to Compton-thin AGN (e.g. Crawford et al. 2002).

If we assume that the $5 - 12$ keV flux density is little affected by absorption then the AGN are characteristic of those found at the break of the X-ray luminosity function ($L\star$) to within a factor of ~ 5. For example, ero5 at $z = 1.45$ has an intrinsic luminosity, $L_X \sim 10^{44.1}$ erg $\mathrm{s^{-1}}$, while ero1 at $z = 3$ would have $L_X \sim 10^{45.2}$ erg $\mathrm{s^{-1}}$ compared to $L\star$ $(z = 2) \sim 10^{44.5}$ erg $\mathrm{s^{-1}}$ (Page et al. 1997). This result implies that four out of five of our EROs contain absorbed AGN with equivalent luminosities to those that make up the bulk of the unobscured component of the extragalactic X-ray background.

The only ERO in our sample that does not appear to have a significant contribution from an AGN is ero3. If it does contain an AGN, then the X-ray spectral fitting suggests that it cannot be absorbed by a significant amount of material. Its diffuse, extended near-infrared morphology, however, shows that such an unabsorbed AGN must be weak, because it makes a negligible contribution to the K-band light. Alternative sources of the X-ray emission are powerful starburst activity or halo emission from a massive elliptical galaxy in a deep gravitational potential. The former case is unlikely for a number of reasons. Firstly, ero3 was undetected in both the submillimetre and radio bands showing that star formation is not occurring on a massive scale; the limit derived from the deep radio map is SFR < 50 $\mathrm{M_{\odot}yr^{-1}}$ at $z = 1$. Secondly, its X-ray flux corresponds to a luminosity $L_X \sim 10^{43.5}$ erg $\mathrm{s^{-1}}$ $(z = 1)$ or $L_X \sim 10^{44.1}$ erg $\mathrm{s^{-1}}$ $(z = 2)$. This luminosity is too large for almost any conceivable starburst; the brightest X-ray starburst known is NGC 3256 with $L_X = 10^{42.4}$ erg $\mathrm{s^{-1}}$ (Moran, Lehnert & Helfand 1999), more than an order of magnitude less luminous than ero3. The temperature that we obtain from the fit to the X–ray spectrum ($\sim$ 1–3 keV, see Fig. 3) and the luminosity

Table 6. Summary of source properties and proposed classification.

Name	Best fit X-ray spectrum	colour diagnostic	K-band size diagnostic	submm/radio SFR ($M_\odot$ yr^{-1})[a]	conclusion
ero1	absorbed power law	starburst	AGN	340	absorbed AGN with starburst.
ero2	absorbed power law	ambiguous	AGN	< 80	absorbed AGN. Quiescent host with circumnuclear torus?
ero3	thermal plasma	elliptical	elliptical	< 50	giant elliptical galaxy
ero4	absorbed power law	elliptical	elliptical	90	absorbed AGN. Quiescent host with circumnuclear torus?
ero5	absorbed power law	starburst	AGN	1500	absorbed AGN with starburst. ULIRG.

[a] SFRs are calculated assuming $z = 1$ except for ero5 which has a measured redshift of $z = 1.45$

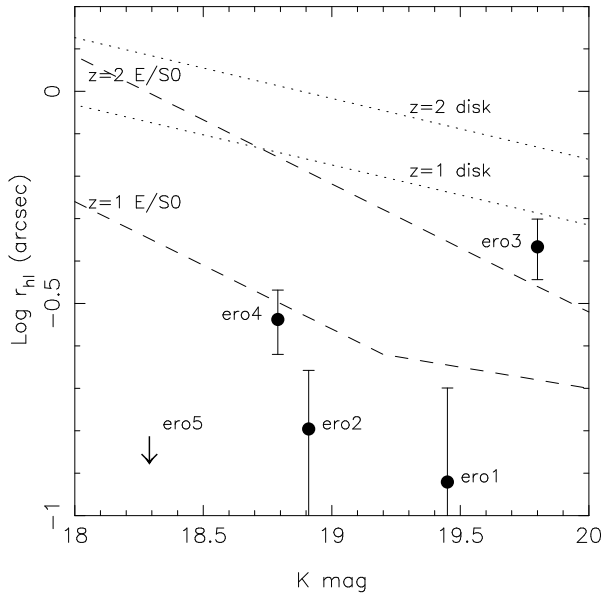

Figure 6. Half-light radii against K magnitude. The dotted and dashed lines are models taken from Roche et al. (2002).

are, however, within the range of values found for cD galaxies locally (O'Sullivan, Forbed & Ponman 2001, Matsushita 2001). This is consistent with the optical/IR colour and size results discussed above and suggests that ERO3 is likely to be the dominant galaxy of a cluster.

These results are in good agreement with those deduced from the *Chandra* Deep Field North Survey (Alexander et al. 2002). They claim that X-ray selected EROs that were detected in the hard band are absorbed AGN (9 out of 13 sources), while the 4 sources detected only in the soft band have X-ray emission from less energetic processes. In particular, a stacking analysis of those EROs with $I < 24.1$ that were not individually detected resulted in a statistical detection in the soft band. They argue that this result is consistent with that expected if the majority of these sources are typical elliptical galaxies. X-ray spectral fitting shows convincingly that 4/5 of our sources are absorbed AGN, and that the other source is likely to be an elliptical galaxy, albeit a very luminous example.

Although our sample is small, two of the absorbed AGN are likely to contain substantial quantities of warm dust. We speculate that the other absorbed AGN might contain only hot circumnuclear dust. These properties are in keeping with the predictions of models for the X-ray background (Fabian & Iwasawa 1999). This result might also suggest that EROs detected as counterparts to faint submillimetre galaxies (e.g. Smail et al. 1999) have a reasonable chance of being associated with AGN, although we have already noted that only ~ 4 per cent of EROs in the Lockman Hole sample are X-ray sources (Section 2). Similarly, Alexander et al. (2002) find that only 14^{+11}_{-7} per cent of the $K \leq 20.1$ ERO population are obscured AGN to the depth of their survey. Another study (Smail et al. 2002) suggests that this number could be as low as 2 per cent although their X-ray data are not as deep as those presented by Alexander et al. (2002). A recent comparison between faint *XMM-Newton* sources and submillimetre galaxies selected from the bright end of the number counts showed an overlap of 4 out of 16, with only one of these sources identified as both an X-ray source and an ERO (Ivison et al. 2002). However, these limits only constrain the fraction of EROs which contain Compton-thin AGN. It will require considerably deeper X-ray observations to detect a population of Compton-thick EROs with X-ray luminosities similar to, or lower than, the 5 EROs studied in this paper.

6 CONCLUSIONS

(i) We present multifrequency follow-up observations and analysis for 5 out of 6 EROs identified in the 100 ks *XMM-Newton* observation of the Lockman Hole. They have enough counts in the X-ray band to allow spectral fitting. Four of them are best-fitted by an absorbed power law model with redshift dependent column densities of $10^{22} - 10^{24}$ cm^{-2}. They are most probably Compton thin, obscured AGN. The fifth source has a best fit thermal spectrum and might be a massive elliptical galaxy with X-ray emission associated with its halo.

(ii) The EROs have optical/near-infrared colours consistent with dusty sources or normal elliptical galaxies. K-band imaging data show that those sources with elliptical colours have sizes predicted for elliptical galaxies at $1 < z < 2$. The other three sources are smaller than the model predictions; it is likely that in these cases the host galaxy is dominated by light from the AGN, consistent with them being Compton-thin AGN.

(iii) The dust content of the EROs is investigated with sensitive observations in the submillimetre and radio bands. Of the two AGN with dusty colours, one of them is detected at 850 μm which we interpret as emission from warm dust heated by young stars. The other is detected at 1.4 and 4.9 GHz suggesting that it also is a galaxy undergoing a burst of star formation, albeit at a less spectacular rate. Of the two sources with elliptical-like colours, one of them (that with the best-fit thermal X-ray spectrum) is undetected in the submillimetre and radio bands. The other is a faint radio source – this radio emission might be attributable to the AGN. We argue that the fifth source, an AGN with an ambiguous colour

classification, has relatively little warm dust, and that the nucleus makes a significant contribution to the K-band light.

(iv) We suggest that the AGN with non-dusty colours might contain hot dust that provides viewing angle dependent obscuration (e.g. a circumnuclear torus), while the dusty AGN might be obscured by warm dust and gas associated with starburst activity. The latter might be in an earlier evolutionary phase than the AGN hosted by quiescent, early type galaxies.

(v) The EROs that host AGN have luminosities within a factor of 5 of those found at the break of the unabsorbed X-ray luminosity function, i.e. they have luminosities equivalent to AGN that make up the bulk of the unobscured X-ray background.

ACKNOWLEDGMENTS

The James Clerk Maxwell Telescope is operated by the Joint Astronomy Centre in Hilo, Hawaii on behalf of the parent organizations PPARC in the United Kingdom, the National Research Council of Canada and The Netherlands Organization for Scientific Research. The United Kingdom Infrared Telescope is operated by the Joint Astronomy Centre on behalf of PPARC. Based on observations obtained with *XMM-Newton*, an ESA science mission with instruments and contributions directly funded by ESA member states and the USA (NASA). NRAO is operated by Associated Universities Inc., under a cooperative agreement with the National Science Foundation. J.A.S. acknowledges support from PPARC. I.R.S. acknowledges support from the Royal Society and the Leverhulme Trust.

REFERENCES

Afonso J., Mobasher B., Chan B., Cram L., 2001, ApJ, 559, L101
Alexander D.M., Vignali C., Bauer F.E., Brandt W.N., Hornschemeier A.E., Garmire G.P., Schneider D.P., 2002, AJ, 123, 1149
Antonucci R., 1993, ARA&A, 31, 473
Barvainis R., Lonsdale C., Antonucci R., 1996, AJ, 111, 1431
Blundell K.M., Rawlings S., Willott C.J., 1999, AJ, 117, 677
Carilli C.L., Yun M.S., 2000, ApJ, 530, 618
Comastri A., Setti G., Zamorani G., Hasinger G., 1995, A&A, 296, 1
Conway R.G., Kellerman K.I., Long R.J., 1963, MNRAS, 125, 261
Crawford C.S., Gandhi P., Fabian A.C., Wilman R.J., Johnston R.M., Barger A.J., Cowie L.L., 2002, MNRAS, 333, 809
Deane J.R., Trentham, N., 2001, MNRAS, 326, 1467
Dey A., Graham J.R., Ivison R.J., Smail I., Wright G.S., Liu M.C., 1999, ApJ, 519, 610
Dunne L., Clements D.L., Eales S.A., 2000, MNRAS, 319, 813
Elbaz D., Flores H., Chanial P., Mirabel I.F., Sanders D., Duc P.-A., Cesarsky C.J., Aussel H., 2002, A&A, 381, L1
Elston R., Rieke G.H., Rieke M.J., 1988, ApJ, 331, 77
Elvis M., et al., 1994, ApJS, 95, 1
Fabian A.C., 1999, MNRAS, 308, 39
Fabian A.C., Iwasawa K., 1999, MNRAS, 303, 34
Fadda D., Flores H., Hasinger G., Franceschini A., Altieri B., Cesarsky C.J., Elbaz D., Ferrando Ph., 2002, A&A, 383, 838
Hasinger G., Burg R., Giacconi R., Schmidt M., Trümper J., Zamorani G., 1998, A&A, 329, 482
Hasinger G., et al., 2001, A&A, 365, L45
Hawarden T.G., Leggett S.K., Letawsky M.B., Ballantyne D.R., Casali M.M., 2001, MNRAS, 325, 563
Holland W.S., et al., 1999, MNRAS, 303, 659
Hughes D.H., Robson E.I., Dunlop J.S., Gear W.K., 1993, MNRAS, 263, 607
Ivison R.J., et al., 2002, MNRAS, 337, 1
Jenness T., Lightfoot J.F., 1998, in eds R. Albrecht, R.N. Hook and H.A. Bushouse, Astronomical Data Analysis Software and Systems VII, A.S.P. Conference Series, Vol. 145, p.216
Kennicutt R.C., 1998, ApJ, 498, 541
Lehmann I., et al., 2001, A&A, 371, 833
Lockman F.J., Jahoda K., McCammon D., 1986, ApJ, 302, 432
Lumb D.H., Warwick R.S., Page M., De Luca A., 2002, A&A, 389, 93
Mainieri V., Bergeron J., Hasinger G., Lehmann I., Rosati P., Schmidt M., Szokoly G., Della Ceca R., 2002, A&A, 393, 425
Matsushita K., 2001, ApJ, 547, 693
Moran E.C., Lehnert M.D., Helfand D.J., 1999, ApJ, 526, 649
Newsam A.M., McHardy I.M., Jones L.R., Mason K.O., 1997, MNRAS, 292, 378
O'Sullivan E.O., Forbes D.A., Ponman T.J., MNRAS, 328, 461
Page M.J., Stevens J.A., Mittaz J.P.D., Carrera F.J., 2001, Science, 294, 2516
Page M.J., Davis S.W., Salvi N.J., 2003, MNRAS, submitted
Page M.J., Mason K.O., McHardy I.M., Jones L.R., Carrera F.J., 1997, MNRAS, 291, 324
Pierre M., et al., 2001, A&A, 372, L45
Pozzetti L., Mannucci F., 2000, MNRAS, 317, L17
Roche N.D., Almaini O., Dunlop J.S., Ivison R.J., Willott C.J., 2002, MNRAS, 337, 1282
Setti G., Woltjer L., 1989, A&A, 224, L21
Smail I., Ivison R.J., Kneib J.-P., Cowie L.L., Blain A.W., Barger A.J, Owen F.N., Morrison G., 1999, MNRAS, 308, 1061
Smail I., Owen F.N., Morrison G.E., Keel W.C., Ivison R.J., Ledlow M.J., 2002, ApJ, 581, 844
Smith G.P., Treu T., Ellis R., Smail I., Kneib J.-P., Frye B.L., 2001, ApJ, 562, 635
Smith G.P., et al., 2002, MNRAS, 330, 1
Wilman R.J., Fabian A.C., Gandhi P., 2000, MNRAS, 318, L11
Yun M.S., Reddy N.A., Condon J.J., 2001, ApJ, 554, 803
Zamorani G., et al., 1994, ApJ, 245, 357

This paper has been typeset from a TEX/ LATEX file prepared by the author.

APPENDIX A: WHAT IS ERO5?

The spectral energy distribution of ero5 is plotted in Fig. A1 where we also show those of the ULIRG ERO J164502+4626.4 otherwise known as HR 10 (Dey et al. 1999) and the dusty quasar ISO J1324−2016 (Pierre et al. 2001), both of which are EROs. The comparison sources, both at $z \sim 1.5$, are plotted in the observed frame, and have not been shifted in flux level. The mid-infrared data are from *ISOCAM* observations of the Lockman Hole which show that ero5 is one of the brightest 15μm sources in the X-ray detected sub-sample (Fadda et al. 2002). There is a striking similarity between ero5 and HR 10 in the millimetre and near-infrared optical regime but ero5 is at least an order of magnitude brighter at radio wavelengths where it is more similar to ISO J1324−2016. The *ISOCAM* data have large uncertainties but nevertheless there is reasonably good evidence that the AGN have rising spectra between the K-band and the mid-infrared whereas the starburst-like HR 10 shows the opposite behaviour.

The millimetre–submillimetre spectral index of > 2.4 practically rules out a self-absorbed synchrotron origin for the submillimetre radiation unless the source varied in between the observations which we consider to be unlikely. Although the spectrum is just consistent with that expected for a homogeneous synchrotron source in the optically thick regime (maximum slope of 2.5) such sources have never been observed with turnovers in the far-infrared

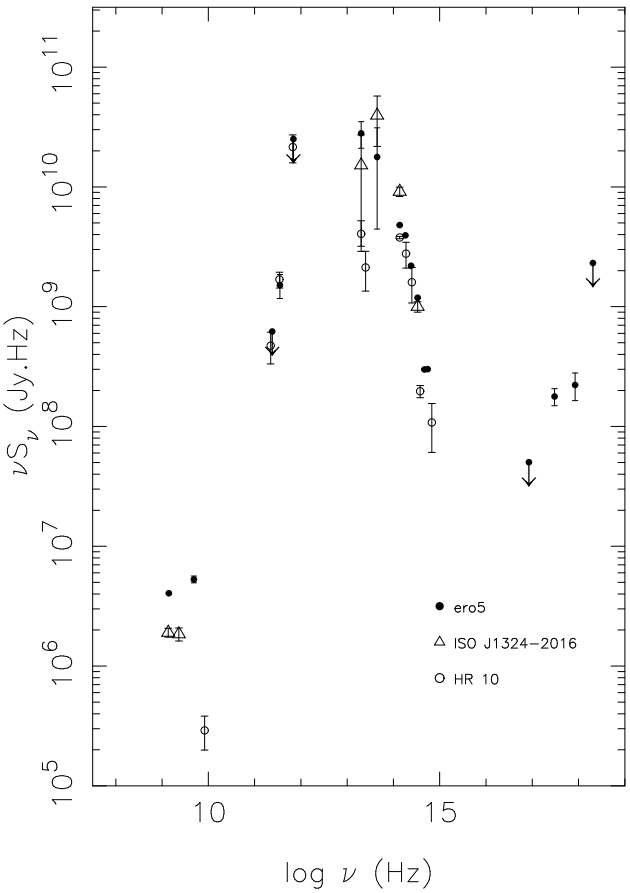

Figure A1. Spectral energy distribution of ero5 plotted for comparison against those of HR 10 (Dey et al. 1999; Elbaz et al. 2002 [mid-infrared]) and ISO J1324−2016 (Pierre et al. 2001). No shifts in absolute flux level have been applied to the data.

(see e.g. discussion in Hughes et al. 1993). The most likely interpretation is thus that the submillimetre flux is due to thermal emission from dust.

The radio emission from ero5 is likely to include a large contribution from the AGN. The spectral index between the radio and submillimetre bands is $\alpha_{1.4}^{350} = 0.07$ which would place the source at $z < 0.3$ if the radio emission is attributed to star formation alone (e.g. Carilli & Yun 1999; Dunne, Clements & Eales 2000). Turning this argument around, and assuming that all of the submillimetre emission is from dusty star formation, the predicted 1.4 GHz flux density in the observer's frame is approximately $30 - 300$ μJy at $z = 1.45$. This result implies that most of the ~ 3 mJy emitted at 1.4 GHz is from processes other than star formation.

Could the source be radio-loud? Our 1.4-GHz radio image constrains the source size to be < 0.5 arcsec. At $z = 1.45$ the projected size must thus be smaller than about 8.6 kpc (or about 12.1 kpc if $q_0 = 0$) if it is to remain unresolved in our radio images. The data presented by Blundell, Rawlings & Willott (1999) show that classical double radio sources have linear sizes ranging from several thousands of kpc to less than one kpc so our size constraints are consistent with a radio galaxy or mis-aligned quasar. Another diagnostic for radio-loudness is the two-point spectral index (α_{ro}) measured in the rest frame between 4.86 GHz and the R-band, where radio-loud sources have indices < -0.35 (Zamorani et al. 1981). We can K-correct the radio data using the observed spectral index between 4.86 and 1.4 GHz of -0.81 ± 0.06, and the observed K-band flux corresponds approximately to the rest frame R-band flux. The calculated index is $\alpha_{ro} = -0.39$ which falls just into the radio-loud regime. However, only 0.5 mags of extinction would be required at K to place the source on the other side of the divide. Given that ero5 is extremely dusty we consider this very likely to be the case, and so it is most probably radio-quiet according to this diagnostic. We note that the observed radio flux density and radio spectral index are consistent with those found for radio quiet quasars (Barvainis, Lonsdale & Antonucci 1996). The emission is probably optically thin synchrotron radiation.